NEAR WAKE STRUCTURE OF A WALL-MOUNTED FINITE-LENGTH SQUARE CYLINDER

H.F. Wang
Department of Mechanical Engineering, the HongKong Polytechnic University, Kowloon, Hong Kong

Y. Zhou
Department of Mechanical Engineering, the HongKong Polytechnic University, Kowloon, Hong Kong

ABSTRACT

This paper reports an experimental investigation of the near wake of a wall-mounted finite-length square cylinder. The height-to-width ratio, H/d (H and d are the cylinder height and width, respectively), of the cylinder is 7. Experiments were conducted at a Reynolds number (Re) of 9300, based on d and the free-stream velocity (U_∞). The PIV measurements were performed in three orthogonal planes in the three-dimensional cylinder wake, along with flow visualization conducted simultaneously in two orthogonal planes at Re = 220. Three types of vortices, i.e. the tip, base and spanwise vortices were observed and the near wake is characterized by the interactions of these vortices. Both flow visualization and two-point correlation point to an inherent connection between the three types of vortices. A model for the 3D flow structure is proposed based on the present measurements, which is distinct from previously proposed models. Other issues such as the topological characteristics, spatial arrangement and interactions among the vortical structures are also addressed.

1. INTRODUCTION

The flow around a nominally two-dimensional (2D) cylinder placed normal to a uniform flow has long been the subject of extensive studies, partially because of its importance in engineering and partially because of its highly organized flow structure, facilitating the study of turbulence. This flow is characterized by the periodic alternate vortex shedding from both sides of the cylinder, forming the Kármán vortex street. A large amount of knowledge about the 2D cylinder wake has been accumulated (e.g., Williamson 1996, Zdravkovich 1997).

In engineering applications, such as pollutant transport around high-rise buildings, plume behaviors behind chimney, aerodynamic forces on cooling towers, etc., the cylinder-like structures often have a limited or finite length (or height), often with one end free and the other fixed on the ground. Naturally, the structures cannot be treated as a 2D cylinder. Due to the end effects, the flow structure behind a finite-length cylinder differs drastically from that behind a 2D cylinder, as unveiled in a number of previous investigations, mostly on circular cylinders (e.g., Etzold & Fielder 1976, Kawamura *et al.* 1984, Okamoto & Sunabashiri 1992, Sumner *et al*. 2004).

The near wake of a wall-mounted finite-length circular cylinder depends strongly on *H/d* (Sakamoto & Arie 1983, Kawamura *et al.* 1984, Okamoto & Sunabashiri 1992 and Summer *et al.* 2004). When *H/d* falls below a critical value $(H/d)_{cr}$, vortex shedding changes from the anti-symmetrical Kármán type to the symmetric arch-type (Sakamoto & Arie 1983, Okamoto & Sunabashiri 1992), and the free-end downwash flow dominates the wake. $(H/d)_{cr}$ is 2 ~ 6, determined by many factors, such as boundary layer thickness and incoming flow turbulence intensity, etc., (Sakamoto & Arie 1983 and Kawamura *et al.* 1984). For $H/d > (H/d)_{cr}$, alternate Kármán vortex shedding occurs along the cylinder span, except near the free end (Kawamura *et al*. 1984, Okamoto & Sunabashiri 1992), where the downwash flow, which is influential, interacts with the Kármán vortices. At $H/d \approx (H/d)_{cr}$, the Kármán-type and arch-type vortices occur intermittently in the near wake (Sakamoto & Arie 1983).

The wake of a wall-mounted finite-length cylinder is characterized by the presence of the longitudinal tip and based vortices, in addition to possible spanwise vortex shedding. The interactions between the three types of vortices complicate the flow and make it highly three dimensional. The tip vortices, associated with the downwash flow from the free end, occur near the free end in the form of a pair of counter-rotating streamwise structures (Etzold & Fiedler 1976, Kawamura *et al*. 1984). Summer *et al*. (2004) measured the time-averaged cross-stream velocity field behind a wall-mounted finite-length circular cylinder, immersed in a boundary layer with a thickness $\delta = 2.6d$, using a 7-hole pressure probe. They observed one pair of streamwise vortices, with the opposite sense to the tip vortices, near the cylinder base, which are

referred to as the base vortices. Both Etzold & Fiedler (1976) and Summer *et al.* (2004) ascribed the formation of the base vortex to the inclined spanwise vortices near the wall. Interestingly, the base vortex is absent when the boundary layer is negligibly thin (Etzold & Fiedler 1976, Okamoto & Sunabashiri 1992), that is, the presence of the base vortex depends on that of the boundary-layer conditions. This is consistent with the finding in a wall-mounted finite-length square cylinder wake that the upwash flow induced by the base vortex is enhanced with the increasing boundary layer thickness (Wang *et al.* 2006).

Despite the studies mentioned above, the near wake structure of a finite-length cylinder has not been thoroughly understood. The present work aims to investigate experimentally the flow around a wall-mounted finite-length square cylinder in order to gain a better understanding of the near wake, in particular, the interrelationship among the tip, base and spanwise vortices. An obvious advantage from investigating the square cylinder rather than the circular is that the flow separation is fixed at the leading edge, thus simplifying the problem concerned. The present examined H/d is 7, which is typical for many engineering structures. The PIV measurements were conducted in three orthogonal plans, along with flow visualization performed simultaneously in two orthogonal planes in order to capture the three dimensional aspects of the flow structure.

2. EXPERIMENTAL DETAILS

PIV and hotwire measurements were conducted in a closed-loop wind tunnel with a 2.4-m-long test section and a cross section of 0.6m × 0.6m. The nonuniformity of streamwise velocity was less than 0.1% and the streamwise turbulence intensity was less than 0.4%. A square cylinder was mounted on a horizontal flat plate to generate the wake, as shown in Figure 1. The leading edge of the flat plate was rounded carefully to avoid flow separation. The square cylinder with a width d = 20mm and H/d = 7 was placed at the centerline, 0.3m downstream from the leading edge of the flat plate. The blockage ratio was 2.2%, thus resulting in a negligible blockage effect. The measurements were conducted at a free-stream velocity $U_\infty \approx$ 7m/s, corresponding to a Reynolds number $\mathrm{Re}_d \equiv U_\infty d/\nu \approx 9300$, where ν is the kinematic viscosity of fluid. A laser Doppler anemometer (LDA) was used to document the boundary layer at the cylinder axis prior the cylinder installation. The boundary layer thickness δ was 27mm, i.e. $\delta/d \approx 1.35$.

A DANTEC standard PIV2100 system was used to measure the flow fields. The flow was seeded by smoke generated from paraffin oil by a smoke generator. Flow illumination was provided by two Newwave standard pulse laser sources of a 532nm wavelength. Synchronization between image taking and flow illumination was provided by the Dantec FlowMap Processor (PIV2001 type). The PIV measurements were performed in three orthogonal planes, i.e. the (x, z)-plane at y^* =0 (the asterisk denotes normalization by U_∞ and/or d), the (x, y)-planes at z^* = 1, 3.5 and 6, and the (y, z)-planes at x^* = 1, 3 and 5. For measurements in each plane, 200 images were captured to calculate time-averaged velocity fields.

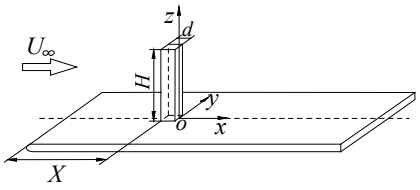

Figure 1: *Experimental setup and the definition of the coordinate system.*

Hotwire was used to measure streamwise fluctuating velocity u to determine the vortex-shedding frequency. It was traversed along the spanwise direction at y^* = 2 and x^* = 3, 5 and 10. The signal was offset, low-pass filtered at a cut-off frequency of 1.5kHz, and then sampled at a frequency of 3kHz. The sampling duration for each record was 20s. In order to obtain the spectral coherence along the cylinder span, measurements were conducted using two hotwires placed at y^* = 2 and x^* = 3, one fixed at z^* = 1 and the other traversed along the cylinder span at an interval of 1d. The signals from the two wires were recorded simultaneously at the same sampling conditions as those used in the single hotwire measurements.

Flow visualization was conducted using laser-induced fluorescence (LIF) technique in a water tunnel with a 2.4-m-long test section and a cross section of 0.3m × 0.6m. The free-stream velocity for flow visualization was 0.01m/s, and the corresponding Re_d = 220. The flow visualization was carried out in the (x, y)-planes at z^* = 1, 3.5 and 6. Flow visualization was also performed simultaneously in two orthogonal planes, i.e., the (x, y)-plane at z^* = 6 and the (x, z)-plane at y^* = 0, in order to capture the three-dimensional aspects of vortical structures emanating from the free end, including interaction between the free-end shear flow and spanwise shear flow. The two planes were simultaneously illuminated using two laser sheets. Two digital video cameras were synchronized using one remote controller, thus ensuring the simultaneous capture of images in the two planes.

3. PIV measurement results

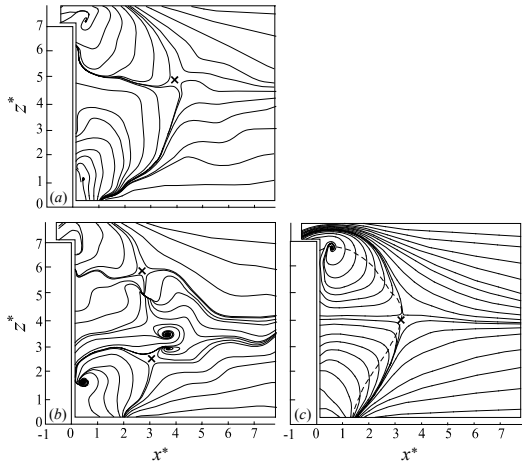

Figure 2: *Typical instantaneous (a, b) and time-averaged (c) sectional streamlines in the (x, z)-plane at y^*=0, viewed from a fixed reference frame.*

Figure 2 shows typical instantaneous and time-averaged sectional streamlines in the (x, z)-plane at $y^* = 0$. Two types of instantaneous streamlines are observed. One is characterized by a downwash flow meeting with an upwash flow from the cylinder base (figure 2*a*). Note that the saddle point, marked by the '×', results apparently from the interaction between the upwash and downwash flows. The other appears more complicated, showing more critical points (e.g. Zhou & Antonia 1994), including two saddle points, three foci and a node (figure 2*b*). The presence of two foci associated with counter-rotating vortical structures is consistent with the occurrence of mushroom-like longitudinal rib structures, as observed by Wu *et al*. (1996) in close proximity to a 2D cylinder. These rib structures are closely associated with spanwise vortex rolls. The observation suggests that the flow topology in figure 2(*b*) is associated with spanwise vortex shedding, while in the case of figure 2(*a*) downwash and upwash flows are predominant, with spanwise vortex shedding absent. The flow about the node is strongly three dimensional, with a large velocity gradient in the y direction (Zhou & Antonia 1994). The presence of the node is probably ascribed to the rollup of spanwise shear layer that sweeps across the central plane ($y^* = 0$). Time-averaged streamlines (figure 2*c*) out of 200 instantaneous images are topologically similar to those in figure 2(*a*), and also to those behind a wall-mounted finite circular cylinder of the same H/d (Summner *et al*. 2004). As noted from instantaneous streamlines, the node and foci in figure 2(*b*) occur rather randomly in time and streamwise location, therefore averaged out, disappearing in the time-averaged streamlines.

The boundary of reversal flow zone, determined from $\overline{U} = 0$ (the overbar denotes time-average), is marked by a thick dash-line in figure 2(*c*). As expected, the size of this zone depends on z^*, largest at the mid-span ($z^* = 3.5$) and smallest near the free end ($z^* = 6$), similarly to previous observations behind a wall-mounted finite-length circular cylinder (Okamoto & Sunabashiri 1992 and Sumner *et al*. 2004). The small size near the free end is apparently caused by the rolling down free-end shear flow (figure 2*c*), which acts to suppress spanwise vortex shedding (Okamoto & Sunabashiri 1992). On the other hand, the small size near the wall is ascribed to the upwash flow from the cylinder base (figure 2*c*), which is also inclined to weakening spanwise vortices (Wang *et al*. 2006).

Because of the limitation of the paper length, the PIV measurement results in the (x, y)-planes at z^* = 1, 3.5 and 6 are not presented here. Although the present H/d = 7 exceeds considerably $(H/d)_{cr}$ (= 3) proposed by Sakamoto & Arie (1983), both symmetrically and anti-symmetrically arranged vortices occur in all presently measured (x, y)-planes, similar to that reported by Wang *et al*. (2006) for a square cylinder with H/d = 5.

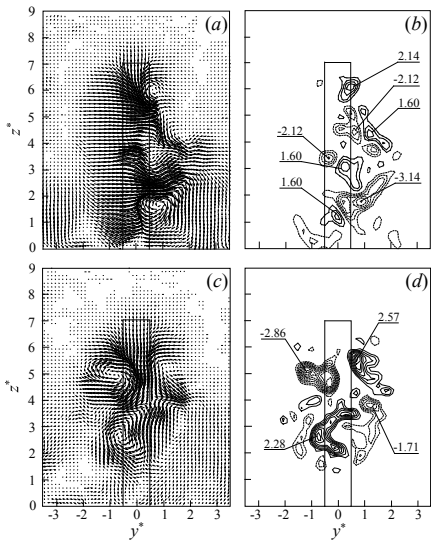

Figure 3: *Instantaneous velocity vectors and the corresponding ω_x^*-contours in the (y, z)-plane at x^* =5, (b) $\Delta\omega_x^*$ = 0.51, (d) 0.28.*

Typical instantaneous cross-stream velocity vectors and the corresponding ω_x^*-contours measured in the (y, z)-plane at $x^* = 5$ are shown in figure 3. The results at x^* =1 and 3 are topologically similar, thus not presented here. Two distinct flow patterns are observed in the (y, z)-plane, and they occur intermittently. When spanwise shear flow sweeps across the central plane, as illustrated in figure 3(*a*), vortical structures, which are probably the signature of longitudinal vortices in the (y, z)-plane, appear on the right-hand side of the cylinder.

These vortical concentrations occur alternatively in sign (figure 3*b*), similar to the rib structures observed in a 2D cylinder wake (Wu *et al*. 1996, Chyu & Rockwell 1996). It may be inferred from these previous observations that the flow pattern shown in figure 3(*a*, *b*) corresponds to the rollup of spanwise shear layer sweeping across the central plane. The other flow pattern, shown in figure 3(*c*, *d*), is characterized by two pairs of counter-rotating vortical structures, one pair near the free end and the other near the wall. Obviously, the former is linked to the downwash flow emanating from the free end and the latter is connected to the upwash flow from the wall, i.e. 'tip vortices' and 'base vortices, respectively. The upwash and downwash flow dominate the whole wake and clash with each other near the cylinder mid-span. It is worth mentioning that, the upwash flow and base vortices cannot be ascribed to the horseshoe vortex formed around the cylinder base, which is characterized by a rollup motion in front of the obstacle, wrapping around from both sides of the cylinder and trailing off behind. The horseshoe vortex tends to drive flow downwards inside its vertical tails (Simpson 2001).

The two distinct flow patterns in the (*y*, *z*)-plane (figure 3) are speculated to associate with the two types of flow structures in the other two planes, i.e. the (*x*, *z*)-plane and the (*x*, *y*)-plane. During Kármán vortex shedding, the spanwise shear layer rolls up and sweeps across the central plane, which is responsible for the presence of a node in the central plane (e.g. figure 2*b*). In view of the association between Kármán vortices and longitudinal structures (Wei & Smith 1986, Wu *et al*. 1996), the alternately signed ω_x^* concentrations (figure 3*b*), which occur on only one side of the cylinder, are the signature of this longitudinal structures in the (*y*, *z*)-plane. On the other hand, in the absence of spanwise Kármán vortex, no shear layer sweeps across the central plane and the node does not occur (figure 2*a*). Furthermore, the near wake is dominated by downwash and upwash flows (figure 3*c*), resulting in symmetrically arranged spanwise vortices in the (*x*, *y*)-plane, and also the simultaneous occurrence of tip and base vortices, symmetrically arranged about the cylinder.

4. Quasi-periodical flow structure and its spanwise coherence

Figure 4 presents the power spectral density function, E_u, of streamwise fluctuation velocity *u* measured using the hotwire. At $x^* = 3$, E_u at the mid-span displays a pronounced peak at $f_s^* = 0.11$, indicating the occurrence of spanwise vortex shedding. This dominant frequency is lower than that in a 2D square cylinder wake, which was reported to be 0.125 ~ 0.13 at Re = $1\times10^3 \sim 2\times10^4$ (Okajima 1982). Zdravkovich (2003) ascribed the decrease in Strouhal number in the finite-length cylinder wake to the free-end downwash flow which elongates the vortex formation length and widen the near wake, thus prolongs spanwise vortex shedding.

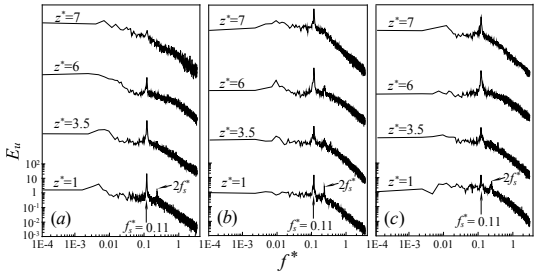

Figure 4: *The power spectra density functions, Eu, of u at y*=2 and (a) x*=3; (b) 5; (c) 10.*

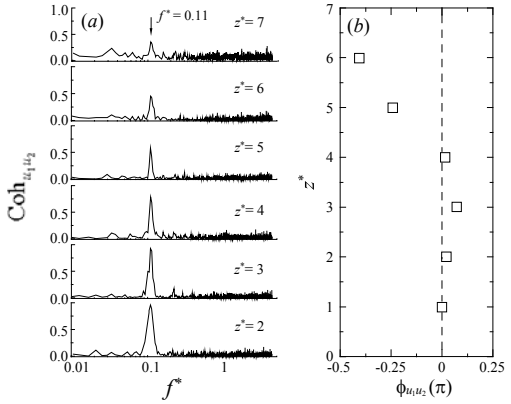

Figure 5: *(a) spectral coherence $Coh_{u_1u_2}$, and (b) phase relation $\phi_{u_1u_2}$ between u_1 and u_2 measured by two hotwires at x*=3 and y*=2, one was fixed at z*=1, the other traversed along z*=2-7.*

The Strouhal number measured at other spanwise locations is identical to that at mid-span. A minor peak occurs at $f^*= 0.22$ at $z^* = 1$ and 3.5, apparently due to the second harmonic of f_s^*. The major peak of E_u appears weak at $z^* = 7$. Apparently due to the downwash flow interacts with and hence weakens spanwise vortex shedding (Okamoto & Sunabashiri 1992). Further downstream at $x^* = 5$ and 10, a pronounced peak occurs at $f^* = 0.11$ for all spanwise locations, including $z^* = 7$ (figure 4*b*, *c*), suggests a weakened downwash flow effect.

Two hotwires were placed at $x^* = 3$ and $y^* = 2$, with one wire fixed at $z^* =1$ and the other traversed along the cylinder span at an interval of 1*d*, from $z^* = 1$ to 7, producing two hotwire signals u_1 and u_2, respectively. The spectral coherence between u_1 and u_2, $Coh_{u_1u_2} = (Co^2_{u_1u_2} + Q^2_{u_1u_2}) \big/ E_{u_1} E_{u_2}$, provides a

measure of the degree of correlation between the two Fourier components of u_1 and u_2. The spectral phase angle $\phi_{u_1u_2}\left(\equiv \tan^{-1}(Q_{u_1u_2}/Co_{u_1u_2})\right)$ gives the information of averaged phase shift between u_1 and u_2, where $Co_{u_1u_2}$ and $Q_{u_1u_2}$ are the cospectrum and quadrature spectrum of u_1, u_2. The $Coh_{u_1u_2}$ exhibits a pronounced peak at $f^* = 0.11$, as shown in figure 5(*a*). This peak value of $Coh_{u_1u_2}$ ranges from more than 0.9 at $z^* = 2$ to about 0.3 at $z^* = 7$, suggesting a significant spanwise correlation of vortex separation throughout the cylinder span. The fact that the f_s^* in E_u occurs at the same frequency throughout the cylinder span and the strong spanwise correlation at all spanwise locations imply that the tip, base and spanwise vortices bear the same frequency, and each of the three vortices may be part of the same entity of the organized structure. Figure 5(*b*) presents the dependence of $\phi_{u_1u_2}$ at $f_s^* = 0.11$ on z^*. There is no data for $\phi_{u_1u_2}$ at $z^* = 7$, because of a very low spectral coherence between u_1 measured at $z^* = 1$and u_2 at $z^* = 7$. It is evident that vortex shedding at the mid span leads in phase, while that near the cylinder free end or wall lags significantly. It seems that, under the effects of downwash flow and boundary layer, the two ends of the spanwise vortex roll leans upstream towards the cylinder free end and the base.

5. Interconnected vortical structures

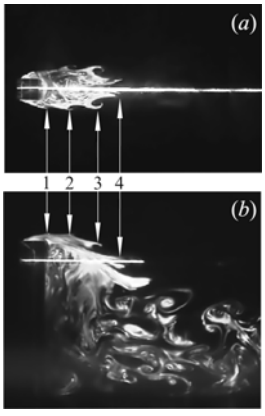

Figure 6: *Images simultaneously captured in : (a) the (x, y)-plane at z^*=6, (b) the (x, z)-plane at y^*=0.*

Flow visualization was conducted at $Re_d = 220$ in order to gain a better understanding of the flow structure. The flow structures were captured simultaneously in the (*x*, *y*)-plane at $z^* = 6$ and the (*x*, *z*)-plane at $y^* = 0$. Figure 6(*b*) shows the rollup and descend of the free-end shear layer. This descending free-end shear layer leads to the disappearance of vortices in the (*x*, *y*)-plane ($z^* = 6$) downstream from the 4th vortex marked in figure 6(*a*). As marked by 1, 2, 3 and 4, there is a nice and neat correspondence between the rollup structures in the spanwise shear layer and free-end shear layer. With simultaneously captured images, this correspondence indicates unequivocally a physical connection between the flow structures in the two planes, that is, each pair of symmetric vortices seen in the (*x*, *y*)-plane and the corresponding rollup structure separating from the free end are part of the same vortical structure, as speculated by Okamoto & Yagita (1973).

The present flow visualization at $Re_d = 220$ shows only the symmetric spanwise vortices at $z^* = 6$ (figure 6*a*), no anti-symmetric vortices at all. This is in distinct contrast with the PIV results, where both symmetrically and anti-symmetrically arranged vortices may occur near the free end at $Re_d = 9300$. The occurrence of anti-symmetric vortices near the free end is apparently due to the turbulence at the higher Reynolds number, which is associated with instability and hence unsteady flow separation.

Flow visualizations was also conducted at $z^* = 3.5$ and 1 (not presented here). Both symmetrical and anti-symmetrical vortices occur intermittently at these locations, consists with the PIV measurements results in the (*x*, *y*)-planes at $Re_d = 9300$.

6. CONCLUSION

Flow around a wall-mounted finite-length square cylinder with $H/d = 7$ has been experimentally investigated. The flow structure was examined in detail, based on Hotwire, PIV and LIF techniques. The experimental results may lead to the following conclusions:

1) The flow behind the finite-length square cylinder is highly three dimensional, largely consisting of free-end downwash flow, spanwise shear flow and upwash flow from the cylinder base, which are associated with the tip, spanwise and base vortices, respectively. The near wake is characterized by interactions between these three components.

2) The same vortex shedding frequency ($f_s^* = 0.11$) and strong spectral coherence at all z^* point to a definitive relationship between the organized structures throughout the entire cylinder span. Each of the three types of vortices may be simply part of a single vortical structure separating from the cylinder. As such, an arch-type flow structure model is proposed in figure 7, where the tip and base vortices separate together, along with spanwise vortex shedding, from the cylinder. The upper half of the arch-type vortex leans upstream against the free end, forming a pair of streamwise vortices, i.e. the tip vortices. The spanwise vortices separated

from both sides of the cylinder are inclined upstream near the wall because of the low speed in the boundary layer, resulting in another pair of streamwise vortices near the wall, i.e. the base vortices.

3) The most representative instantaneous spatial configurations of the oppositely signed vortices observed in the (x, y)-plane are anti-symmetrical and symmetrical. When spanwise shear flow is subdued, spanwise vortices tend to occur symmetrically about the center line. Meanwhile, the longitudinal tip and base vortices tend to be symmetrical about the wake central plane, as shown in figure 7(a). On the other hand, when the spanwise shear sweeps across the wake central plane, the oppositely signed vortical structures in the (x, y)-plane will be anti-symmetrically arranged, with both tip and base vortices invisible in the (y, z)-plane at the side of the spanwise shear flow, as shown in figure 7(b).

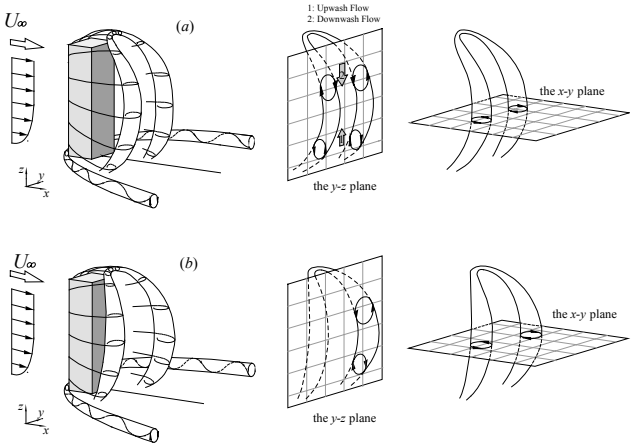

Figure 7: *Model of the flow structure around a wall-mounted finite-length square cylinder: (a) symmetrical status; (b) anti-symmetrical status.*

7. REFERENCES

Chyu. C. & Rockwell. D. 1996 Evolution of patterns of streamwise vorticity in the turbulent near wake of a circular cylinder. *J. Fluid Mech*. **320**: 117-137.

Etzold, F. & Fiedler, H. 1976 The near-wake structure of a cantilevered cylinder in a cross-flow. *Z. Flugwiss* **24**: 77-82.

Kawamura, T., Hiwada, M., Hibino, T., Mabuchi, I. & Kumada, M. 1984 Flow around a finite circular cylinder on a flate plate. *Bull. JSME* **27**: 2142-2150.

Lyn, D.A., Einav, S.E., Rodi, W. & Park, J.H. 1995 A laser-Doppler velocimetry study of ensemble-averaged characteristics of the turbulent near wake of a square cylinder. *J. Fluid Mech*. **304:** 285-319.

Okajima, A. 1982 Strouhal numbers of rectangular cylinders. *J. Fluid Mech*. **123**, 379-398.

Okamoto, T. & Sunabashiri, Y. 1992 Vortex shedding from a circular cylinder of finite length placed on a ground plane. *J. Fluids Eng*. **114**: 512-521.

Okamoto, T. & Yagita, M. 1973 The experimental investigation on the flow past a circular cylinder of finite length placed normal to the plane surface. *Bull. JSME* **16**: 805-814

Sakamoto, H. & Arie, M. 1983 Vortex shedding from a rectangular prism and a circular cylinder placed vertically in a turbulent boundary layer. *J. Fluid Mech.* **126**: 147-165

Simpson, R.L. 2001 Junction Flow. *Annu. Rev. Fluid Mech*. **33:** 415-443.

Summer, D., Heseltine, J.L. & Dansereau, O.J.P. 2004 Wake structure of a finite circular cylinder of small aspect ratio. *Exp. Fluids* **37**: 720-730.

Wang. H.F., Zhou, Y., Chan, C.K. & Lam, K.S. 2006 Effect of initial conditions on interaction between a boundary layer and a wall-mounted finite-length-cylinder wake. *Phys. Fluids*, **18:** 065106

Wei, T. & Smith, C.R. 1986 Secondary vortices in the wake of circular cylinders. *J. Fluid Mech.* **169**: 513-533.

Williamson, C.H.K. 1996 Vortex dynamics in the cylinder wake. *Annu. Rev. Fluid Mech*. **28**, 477-539.

Wu, J., Sheridan, J., Welsh, M.C. & Hourigan, K. 1996 Three-dimensional vortex structures in cylinder wake. *J. Fluid Mech*. **312**: 201-222.

Zdravkovich, M.M. 1997 Flow around circular cylinders, vol 1: Fundamentals. Oxford University Press, Oxford.

Zdravkovich, M.M. 2003 Flow around circular cylinders, vol 2: Applications. Oxford University Press, Oxford.

Zhou, Y. & Antonia, R.A. 1994 Critical points in a turbulent near wake. *J. Fluid Mech*. **275:** 59-81.